Lag-twist coupling sensitivity and design for a composite blade cross-section with D-spar

M.R. Amoozgar *, A.D. Shaw, J. Zhang, C. Wang, M.I. Friswell

College of Engineering, Swansea University, Swansea SA1 8EN, United Kingdom

ABSTRACT

In this paper, the effect of various parameters of a specific rotor blade cross-section on the effectiveness of a twist morphing concept is investigated. Then, by considering different constraints, a cross-section consistent with this morphing concept with high lag-twist coupling and low extension-twist, is developed. This lag bending-torsion coupling is used to change the twist of the blade during the flight, while the high values of extension-twist coupling is avoided. To this end, a concentrated mass is added to the blade, where its chordwise location varies in flight. When the mass moves in the chordwise direction, a local lag bending is introduced into the blade. This in-plane bending moment then changes the blade twist distribution through lag-twist coupling induced through stiffness tailoring in the blade cross-section. Therefore, this coupling plays an important role in this morphing concept. The one-dimensional dynamics of the blade is modelled by using the geometrically exact fully intrinsic bean equations while the 2D cross-sectional stiffness values are determined by using the VABS software. First, a blade which resembles the BO-105 main rotor blade in the fundamental frequencies is designed. Then, the effect of various parameters of the cross-section on the fundamental frequencies, the lag-twist coupling, and the extension-twist coupling are determined. It is found that the skin of the spar has the highest contribution to both the extension-twist and the lag-twist coupling. Finally, a cross-section compatible with the proposed morphing concept is designed and it is demonstrated that the twist of the blade may be changed significantly.

© 2019 Elsevier Masson SAS. All rights reserved.

1. Introduction

The blade twist affects the helicopter induced power, and the twist distribution of the blade should be is an important factor in performance. Generally, the twist distribution of the blade is a compromise between hover and forward flight as the optimal twist requirement for these two flight regimes are different. Changing the twist of the blade in flight has the potential to improve the performance of the rotorcraft. The optimum twist of the blade is a function of disc loading and blade tip Mach number [1]. The twist morphing concept has achieved intense interest from many authors for both fixed and rotary wing aircraft [2]. There are several studies concerned with the twist morphing of fixed-wing aircraft. Vos et al. [3] introduced a concept which is able to change the twist of the wing by warping the wing skin which is an open section due to a split skin at the trailing edge. Changing the twist distribution of the wing by using the bending-torsion coupling of the section was investigated by Raither et al. [4]. In this study

by moving the shear centre from the centroid of the section, a bending-torsion coupling is introduced to the system. Jenett et al. [5] described a new approach to assemble deformable structures by using modular building blocks. In this way, the main structure of the wing is built through some discrete lattice parts which can be used to create meta-materials.

Apart from the application of twist morphing to fixed-wings, several attempts were carried out on the application of twist change to rotary-wings. Initially the idea of changing the twist of the blade was introduced for vibration reduction. Chen and Chopra [6,7] changed the twist a blade by the application of the piezoelectric actuators. It was shown that by distributing the piezoelectric patches on the lower and upper surfaces of the blade skin, about 0.4° twist change is achievable. They also showed that if the blade twist changes linearly by about 0.6°, the rotor lift can be increased by about 10%. The dynamic characteristics of active rotor blades equipped with an active twist mechanism was considered by Cesnik et al. [8]. The obtained results showed that the correlation between the experimental results and the analytical results is good. This study mainly concerned hover flight, and then was extended to the forward flight condition [9]. Thakkar and Ganguli [10] introduced a new analytical model capable of modelling the blades

* Corresponding author.
E-mail address: m.amoozgar@swansea.ac.uk (M.R. Amoozgar).

with piezoelectric material. They highlighted that using the shear actuation devices is more advantageous over the bending actuators in terms of the rotor response. Changing the twist of a tiltrotor blade by application of a torque tube made of shape memory alloys was developed by Prahlad and Chopra [11]. It was determined that the heat treatment of the torque tube influences the actuation behaviour. An active twist rotor blade made of shape memory alloys was tested by Bushnell et al. [12]. Pagano et al. [13] developed a twist morphing concept for a helicopter rotor blade based on using a SMA rod. Twist morphing of rotor blades by using by a warp-induced concept was proposed by Mistry et al. [14]. In this paper, the skin of the blade is warped by using a threaded rod attached to the skin. The effect of blade dynamic twist change on the helicopter flight performance has been investigated by Han et al. [15]. They showed that the lower harmonic twist can reduce the required power more than the higher harmonic twist.

Amoozgar et al. [16–18] proposed a concept that is able to change the twist of a composite blade. In this concept, a movable mass was added to blade which can create an additional torsional moment through the lag-twist coupling of the composite layup. This added mass is used as an actuator to morph the blade and change the twist. It was also highlighted that the value of the lag-twist coupling of the cross-section is very important, and it is crucial to design a cross-section with high coupling. Therefore, in the current study, the main objective is to determine which parts of the blade cross-section are dominant in this lag-twist coupling.

Rotor blade design is a multidisciplinary task which is a compromise between dynamics, aerodynamics, and structures [19]. The blade structural design can be divided into local and global levels [20]. At the global level, the overall shape of the blade, which generally can be selected as a result of the mutual interaction between the aerodynamics, aeroelasticity, and acoustics, is obtained. At the local level, the cross-section of the blade and the material of the structure is determined. Li et al. [20] developed a new systematic methodology for designing the cross-sectional of composite rotor blades based on various constraints. In this study, a sensitivity analysis was carried out to evaluate the effect of thickness, ply angle and location of different components of the cross-section on the various properties. It is noted that in this study, the effect of composite couplings wasn't considered, and therefore in the current study this is investigated. A framework to design an active twist rotor blade integrated with anisotropic piezocomposite actuators was proposed and used for optimizing a cross-section to maximize the twist actuation of the blade by Cesnik et al. [21]. Glaz et al. [22] introduced a new approach based on a surrogate model to design the cross-section of a helicopter blade with lower levels of vibration. The effect of the skin thickness and fibre orientation of a two cell box section on the aeroelasticity of helicopter blades was studied by Ganguli and Chopra [23]. Volovoi et al. [24] considered a D shape spar for a cross-section of a helicopter blade with variable thicknesses, ply angles, and spar location to maintain some specific characteristics of the blade. Paik et al. [25] used the VABS cross-sectional tool for the first time to design the layout of composite blade cross-section. This procedure has been developed further and used for frequency placement for designing a rotor with four blades [26,27]. Vu et al. [28] described a framework that couples the performance, aerodynamic, and structure to the configuration and manufacturing aspects to optimize rotor blades. Several tools were implemented in the process to consistently design a optimal configuration based on a multidisciplinary design optimization algorithm.

In the current study, a composite blade cross-section which is consistent with the twist morphing concept proposed earlier [16–18] is developed. First a baseline blade that resembles the BO-105 main rotor blade is developed, and then the various parameters of the cross-section are defined so that the highest pos-
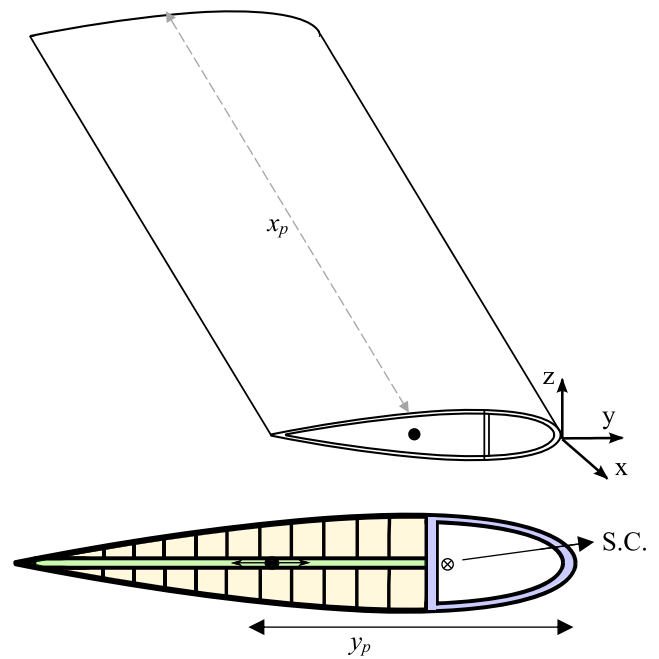

Fig. 1. Schematic of the twist morphing concept with coordinates located at the datum point (0,0,0).

sible lag-twist coupling is achieved with respect to several constraints. The geometrically exact fully intrinsic beam equations are coupled to a cross-sectional analysis tool (VABS) [29]. Then a parametric D-spar cross-section which contains several design variables is introduced, and the effect of each design variable on the extension-twist and lag-twist coupling is evaluated. Finally, a suitable cross-section optimised for this twist morphing concept is designed.

2. Problem statements

A composite hingeless rotor blade as shown in Fig. 1 is considered. The blade is rotating with a constant angular velocity and the cross-section of the blade is composed of a D shape spar. A point mass is added to the blade which can be moved in the chordwise direction by a mechanism. The length of the blade is R, the point mass value is m_p, and its location is determined by x_p, y_p, z_p.

By translating the added mass in flight, a local bending moment is produced on the spar due to the offset between the centrifugal mass acting on the mass and the shear centre of the blade. This bending moment can change the twist of the blade if the cross-section of the blade can produce the lag-twist coupling [16]. Therefore, a proper design of the cross-section is crucial for this morphing concept. Thus, the parametric cross-section shown in Fig. 2 is considered in this study.

The NACA0012 airfoil section is used here to fit the structural parameters. The cross-section is composed of different parts, and the rear part behind the spar web is filled with a light foam. Different cross-sectional design variables with their ranges are defined in Table 1. There are 15 design variables that could be changed during the optimization process. The skin is assumed to be composed of two layers of equal thickness, each composed of a single ply angle, and both the front and back parts of the D-spar have 5 layers with different ply angles. The objective is to design a cross-section subjected to some constraints and having a high value of sectional lag-twist coupling values.
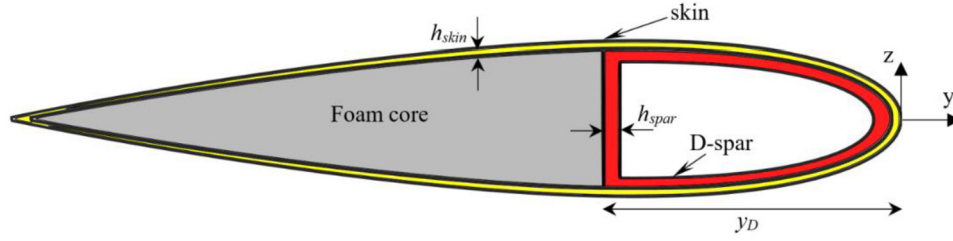
Fig. 2. The parametric cross-section of the blade.

Table 1
The design variables and the design ranges.

Variable name	Design variable	Variable No.	Variable range
skin ply angle (deg)	ζ_1-ζ_2	1-2	[-90,90]
D-spar front part ply angle (deg)	ζ_3-ζ_7	3-7	[-90,90]
D-spar back part ply angle (deg)	ζ_8-ζ_{12}	8-12	[-90,90]
D-spar location (mm)	y_D	13	[-100,-45]
Skin thickness (mm)	h_{skin}	14	[0.5,2]
D-spar thickness (mm)	h_{spar}	15	[1,7]

3. Formulation

The overall dynamics of the composite hingeless rotor blade is simulated by the geometrically exact fully intrinsic beam equations [30], which has been used successfully to model beam-like structures [31–35]. These equations

$$\partial F_1/\partial x_1 + K_2 F_3 - K_3 F_2 = \partial P_1/\partial t + \Omega_2 P_3 - \Omega_3 P_2$$

$$\partial F_2/\partial x_1 + K_3 F_1 - K_1 F_3 = \partial P_2/\partial t + \Omega_3 P_1 - \Omega_1 P_3$$

$$\partial F_3/\partial x_1 + K_1 F_2 - K_3 F_1 = \partial P_3/\partial t + \Omega_1 P_2 - \Omega_2 P_1$$

$$\partial M_1/\partial x_1 + K_2 M_3 - K_3 M_2 + 2\gamma_{12} F_3 - 2\gamma_{13} F_2$$
$$= \partial H_1/\partial t + \Omega_2 H_3 - \Omega_3 H_2 + V_2 P_3 - V_3 P_2$$

$$\partial M_2/\partial x_1 + K_3 M_1 - K_1 M_3 + 2\gamma_{13} F_1 - (1 + \gamma_{11}) F_3$$
$$= \partial H_2/\partial t + \Omega_3 H_1 - \Omega_1 H_3 + V_3 P_1 - V_1 P_3$$

$$\partial M_3/\partial x_1 + K_1 M_2 - K_2 M_1 + (1 + \gamma_{11}) F_2 - 2\gamma_{12} F_1 \qquad (1)$$
$$= \partial H_3/\partial t + \Omega_1 H_2 - \Omega_2 H_1 + V_1 P_2 - V_2 P_1$$

$$\partial V_1/\partial x_1 + K_2 V_3 - K_3 V_2 + 2\gamma_{12}\Omega_3 - 2\gamma_{13}\Omega_2 = \partial\gamma_{11}/\partial t$$

$$\partial V_2/\partial x_1 + K_3 V_1 - K_1 V_3 - (1 + \gamma_{11})\Omega_3 + 2\gamma_{13}\Omega_1 = 2\partial\gamma_{12}/\partial t$$

$$\partial V_3/\partial x_1 + K_1 V_2 - K_2 V_1 + (1 + \gamma_{11})\Omega_2 - 2\gamma_{12}\Omega_1 = 2\partial\gamma_{13}/\partial t$$

$$\partial\Omega_1/\partial x_1 + K_2\Omega_3 - K_3\Omega_2 = \partial\kappa_1/\partial t$$

$$\partial\Omega_2/\partial x_1 + K_3\Omega_1 - K_1\Omega_3 = \partial\kappa_2/\partial t$$

$$\partial\Omega_3/\partial x_1 + K_1\Omega_2 - K_2\Omega_1 = \partial\kappa_3/\partial t$$

where F_i and M_i for $i = 1,..,3$, are the internal forces and moments, V_i and Ω_i are the linear and angular velocities, and P_i and H_i are the sectional linear and angular momenta. The generalized strains of the blade are denoted by γ_{1i} and κ_i, and the final curvature value of the deformed blade is denoted by K_i which is related to the beam curvature as follows

$$K_i = \kappa_i + k_i \qquad (2)$$

where, k_i for $i = 1,..,3$ contain the values of the initial curvature and twist of the blade in the undeformed coordinate.

It is noted that, to derive the intrinsic equations of the beam, the three-dimensional strain energy is solved for the warping, and the asymptotically correct one-dimensional variables are obtained through a rigorous dimensional reduction [30].

The cross-sectional stiffness matrix which relates the internal forces and moments to the generalized strains is obtained by using the cross-sectional analysis software, VABS (ver.3.7.1), which has been extensively validated and used in composite beam applications [29]. The stiffness matrix is defined as

$$\begin{bmatrix} F_1 \\ F_2 \\ F_3 \\ M_1 \\ M_2 \\ M_3 \end{bmatrix} = \begin{bmatrix} S_{11} & S_{12} & S_{13} & S_{14} & S_{15} & S_{16} \\ S_{12} & S_{22} & S_{23} & S_{24} & S_{25} & S_{26} \\ S_{13} & S_{23} & S_{33} & S_{34} & S_{35} & S_{36} \\ S_{14} & S_{24} & S_{34} & S_{44} & S_{45} & S_{46} \\ S_{15} & S_{25} & S_{35} & S_{45} & S_{55} & S_{56} \\ S_{16} & S_{26} & S_{36} & S_{46} & S_{56} & S_{66} \end{bmatrix} \begin{bmatrix} \gamma_{11} \\ 2\gamma_{12} \\ 2\gamma_{13} \\ \kappa_1 \\ \kappa_2 \\ \kappa_3 \end{bmatrix} \quad \text{or}$$

$$\begin{bmatrix} \boldsymbol{F} \\ \boldsymbol{M} \end{bmatrix} = [\boldsymbol{S}] \begin{bmatrix} \boldsymbol{\gamma} \\ \boldsymbol{\kappa} \end{bmatrix} \qquad (3)$$

Among all the components defined in the stiffness matrix, the S_{14} and S_{46} terms, which are extension-twist and lag-twist couplings, are of great importance. This is because they both influence the twist variation of the blade. The extension-twist coupling affects the twist distribution because of the centrifugal force, while the lag-twist coupling changes the twist because of the local bending moment produced by the added mass. Therefore, in this study, both of these couplings are considered and analysed to see which parts of the proposed cross-section can affect them. It is noted that, in this study, the objective is to design a cross-section with high lag-twist coupling and low extension-twist coupling, as the extension-twist coupling may produce high values of adverse twist due to the high centrifugal force acting on the blade. It is noted that as the centrifugal force acting on the blade is high, therefore the extension-twist coupling may produce relatively high twist change on the blade when the blade reaches to its maximum rotating speed. Hence, in this paper to avoid this case, the amount of extension-twist coupling is limited so that when the blade reaches to it its nominal rotating speed, the tip twist of the blade doesn't go higher than -5 degree. This is because that the baseline blade has a pre-twist angle which results to a tip twist value of -5 degree when the blade reaches to its nominal rotating speed.

To close the composite blade formulations, the following boundary conditions are considered:

$$F_{1,2,3}(R,t) = 0, \quad M_{1,2,3}(R,t) = 0, \quad V_{1,2,3}(0,t) = 0,$$

$$\Omega_{1,2}(0,t) = 0, \quad \Omega_3(0,t) = \Omega_0$$

Table 2
The values of the CST function coefficients.

Coefficient	value	Coefficient	value
A_{l0}	0.1718	A_{u0}	-0.1781
A_{l1}	0.15	A_{u1}	-0.15
A_{l2}	0.1624	A_{u2}	-0.1624
A_{l3}	0.1211	A_{u3}	-0.1211
A_{l4}	0.1671	A_{u4}	-0.1671
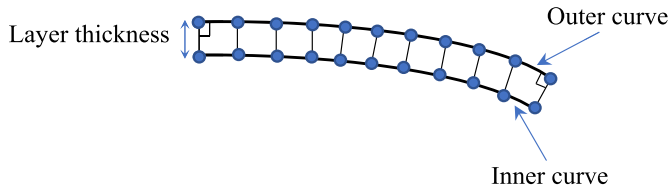
Fig. 3. The construction of the outer and inner curves of each layer.

Table 3
Parameters of the BO-105 main rotor blade.

Item	Value
Radius (R)	4.9 (m)
Chord	0.27 (m)
Pre-cone angle	2.5 (deg)
Rotating velocity (Ω_0)	44.4 (rad/s)
ω_{1_L}	0.66 (/rev)
ω_{1_F}	1.12 (/rev)
ω_{1_T}	3.6 (/rev)

Table 4
Material properties of the skin, spar, and back part of the cross-section.

property	T300/5208	Foam (Rohacell 51 FX)
E_{11} GPa	181	0.035
$E_{22} = E_{33}$ GPa	10.3	0.035
$G_{12} = G_{13}$ GPa	7.2	0.014
G_{23} GPa	3.9	0.014
$\nu_{12} = \nu_{13}$	0.28	0.25
ν_{23}	0.33	0.25
ρ kg/m^3	1600	52

4. Results and discussion

In order to assess the sensitivity of various cross-sectional design variables on the extension-twist coupling and lag-twist coupling, a baseline rotor blade is reproduced for ease of comparison. The baseline cross-section is generated so that the blade resembles the main rotor blade of the BO-105. This baseline blade is assumed to have uniform spanwise properties and it is designed to have fundamental frequencies as closely as possible to the BO-105 blade. To achieve this aim, a generic algorithm optimization is used to determine the design parameters of the cross-section. The cross-section of the blade is meshed adaptively with respect to the design variables. To generate different layers of the cross-section, the inner and outer curves of each layer are represented by means of the Class Function Transformation (CST) [28]. The CST representation of the NACA 0012 airfoil for the upper and lower curves of the airfoil will be

$$\bar{z}_l(x) = \left[\sqrt{\bar{y}}\left(1-\bar{y}\right)\right]\left[A_{l0}(1-\bar{y})^4 + A_{l1}4\bar{y}(1-\bar{y})^3\right.$$
$$\left. + A_{l2}6\bar{y}^2(1-\bar{y})^2 + A_{l3}4\bar{y}^3\left(1-\bar{y}\right) + A_{l4}\bar{y}^4\right]$$
$$\bar{z}_u(x) = \left[\sqrt{\bar{y}}\left(1-\bar{y}\right)\right]\left[A_{u0}(1-\bar{y})^4 + A_{u1}4\bar{y}(1-\bar{y})^3\right.$$
$$\left. + A_{u2}6\bar{y}^2(1-\bar{y})^2 + A_{u3}4\bar{y}^3\left(1-\bar{y}\right) + A_{u4}\bar{y}^4\right]$$

where $\bar{y}$ and $\bar{z}$ are the nondimensional coordinates along the chord and thickness of the airfoil. The constant coefficients ($A_{l0}, \ldots, A_{u4}$) are defined in Table 2.

The CST representation defines the outer curve of each layer. The inner curve of each layer is obtained by translating each point of the outer equal to the thickness of the layer curve normal to the outer curve (Fig. 3).

It is noted that sometimes by applying this procedure, the transformed points may cross each other, and in this case, these points are simply removed from the mesh. However, in the specified range of design variables in this study, this condition rarely happens. The layout and the generated mesh of the cross-section is shown in Fig. 4.

4.1. Baseline design

In this section, the cross-section of the baseline blade is designed so that the fundamental frequencies of the baseline blade are as close as possible to the BO-105 main rotor blade. The BO-105 main rotor blade characteristics are summarized in Table 3.

The spar and skin are made of composite material, and the rear part of the spar is filled with Rohacell 51 FX foam. The material properties used in this study are summarized in Table 4.

At first, the baseline cross-sectional properties are selected by the GA method so that the fundamental frequencies are as close as possible to the BO-105 blade. To achieve this aim, the following constraints are selected

$$0.60/\text{rev} \le \omega_{1_L} \le 0.80/\text{rev}$$
$$1.02/\text{rev} \le \omega_{1_F} \le 1.20/\text{rev}$$
$$3.0/\text{rev} \le \omega_{1_T} \le 4.0/\text{rev}$$
$$0.0 \le |\beta| = \left|\frac{S_{14}}{\sqrt{S_{44}.S_{11}}}\right| \le 0.2$$

where β is the nondimensional extension-twist coupling. There are four constraints, three of which are for the fundamental frequencies, and one is for the nondimensional extension-twist coupling. The extension-twist coupling is bounded, since if this coupling gets very high, it results in high twist values because of the high centrifugal force acting on the blade.

The obtained design variables for the baseline blade with its fundamental frequencies are presented in Tables 5 and 6, respectively. The mass per unit length of the baseline blade is 2.76 kg/m. As the mass per unit length of the BO-105 is about 5.5 kg/m, about 2.74 kg/m mass is added to the blade 5% ahead of the quarter chord to locate the mass centre of the blade in the quarter chord of the section. Furthermore, the elastic axis of the baseline blade is 3.4% ahead of the quarter chord of the blade.

As mentioned earlier, in this twist morphing concept, the lag-twist coupling (S_{46}) plays the main role. Therefore, in this section,

Fig. 4. The mesh and layout of the cross-section.

Table 5
Baseline blade design variables.

Design variable	Value
ζ_1	70°
ζ_2	-83°
ζ_3	0°
ζ_4	-32°
ζ_5	35°
ζ_6	-70°
ζ_7	81°
ζ_8	-67°
ζ_9	-26°
ζ_{10}	86°
ζ_{11}	-73°
ζ_{12}	46°
h_{skin}	1.13 mm
h_{spar}	5.9 mm
y_D	-71.1 mm

Table 6
Comparison of the fundamental frequencies of the baseline design and the BO-105 blade.

Mode	BO-105	Baseline design
ω_{1_L} (/rev)	0.66	0.63
ω_{1_F} (/rev)	1.12	1.04
ω_{1_T} (/rev)	3.6	3.8

the aim is to design a cross-section which is capable of producing lag-twist coupling subjected to the previous constraints. Amoozgar et al. [16] showed that the lag-twist coupling could change the twist distribution of the blade by translating the added mass in the chordwise direction. In this study a nondimensional lag-twist coupling ($\alpha = \frac{S_{46}}{\sqrt{S_{44} \cdot S_{66}}}$) is used to represent the lag-twist coupling value, and the objective is to maximize this variable to be as high as it is possible. This value shows the relation between the lag-twist coupling, and the torsional, and the lag bending stiffnesses.

Before moving to the design of the section with the mentioned properties, it is necessary first to check which part of the cross-section contributes most to the extension-twist coupling and the lag-twist coupling. However, it is also vital to examine which part of the cross-section influences the fundamental frequencies of the blade most significantly. Therefore, in what follows, the sensitivity of each design variable on different parameters are considered.

4.2. Sensitivity analysis

The twist distribution of the blade when there is no added mass on the blade depends on the extension-twist coupling, while when the mass is added to the blade, the lag-twist coupling dominates. Therefore, both couplings are important to be considered to design an optimised cross-section. In this section, the effect of various cross-section design variables on the couplings and fundamental frequencies are evaluated.

The sensitivity of the nondimensional lag-twist coupling to each design variable is shown in Fig. 5. For the whole range of design variables specified in Table 1, the cross-sectional analysis has been carried out by fixing all variables to the baseline blade except the one under consideration. The sensitivity for each design variable, denoted S_i, is determined by

$$S_i = \max\big(H(D_i)\big) - \min\big(H(D_i)\big), \quad i = 1, 2, .., 15$$

where H is the extension-twist or lag-twist value as a function of each design variable in turn. The complete function for all design variables is given by

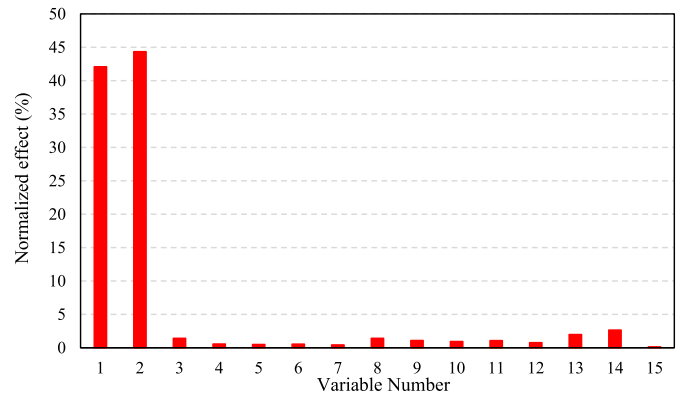$$H = H(D_1, D_2, \ldots, D_{15}), \quad D_{i_{min}} \leq D_i \leq D_{i_{max}}, \quad i = 1, 2, .., 15$$

Fig. 5. The effect of various cross-section design variables defined in Table 1 on the nondimensional lag-twist coupling.
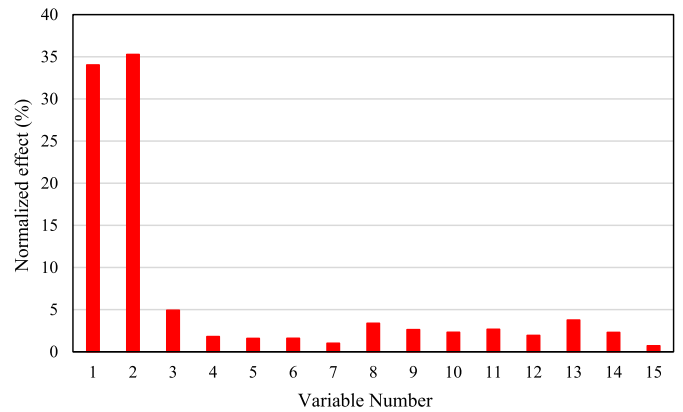

Fig. 6. The effect of various cross-section design variables defined in Table 1 on the nondimensional extension-twist coupling.

where the D_i's are design variables, and $D_{i_{min}}$ and $D_{i_{max}}$ define the minimum and maximum values of each design variable range, respectively. The normalized value of each sensitivity, Γ_i, is then

$$\Gamma_i = \frac{S_i}{\sum_{i=1}^{15} S_i}$$

The length of each bar represents the normalized contribution of each parameter to the coupling in the range of design variables mentioned in Table 1. It is clear that all the design variables influence the lag-twist coupling to some extent, but the main contribution belongs to the ply angles of the first and second layers of the skin (ζ_1 and ζ_2).

Furthermore, the effect of the cross-section parameters on the nondimensional extension-twist coupling is shown in Fig. 6. Again, all the parameters affect this coupling, but the skin ply angles have the highest contribution. By considering both these plots, it is clear that by changing the skin ply angles it may be possible to optimize the lag-twist coupling, however care must be taken as the skin ply angle also can change the extension-twist coupling which is unwanted in this morphing design.

Fig. 7 shows the mutual effect of the ply angles of the first and second layers of the cross-section skin on the nondimensional lag-twist coupling. The skin ply angles affect the coupling significantly, and there is a certain region where the coupling value is maximum for this configuration. For this specific cross-section, the range of the lag-twist coupling value varies between $-0.44 < \alpha < 0.3$. There is a certain range of ply angles at which the maximum absolute values of lag-twist coupling are obtained.

This analysis has been repeated for the nondimensional extension-twist coupling in Fig. 8. For this cross-section, the range of the
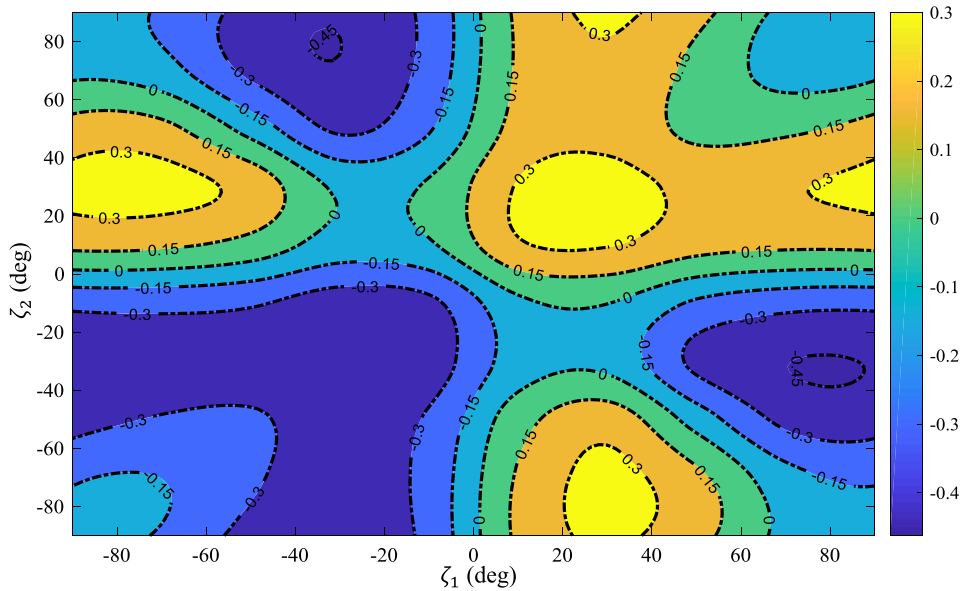
Fig. 7. Mutual effects of ζ_1 and ζ_2 on the nondimensional lag-twist coupling.
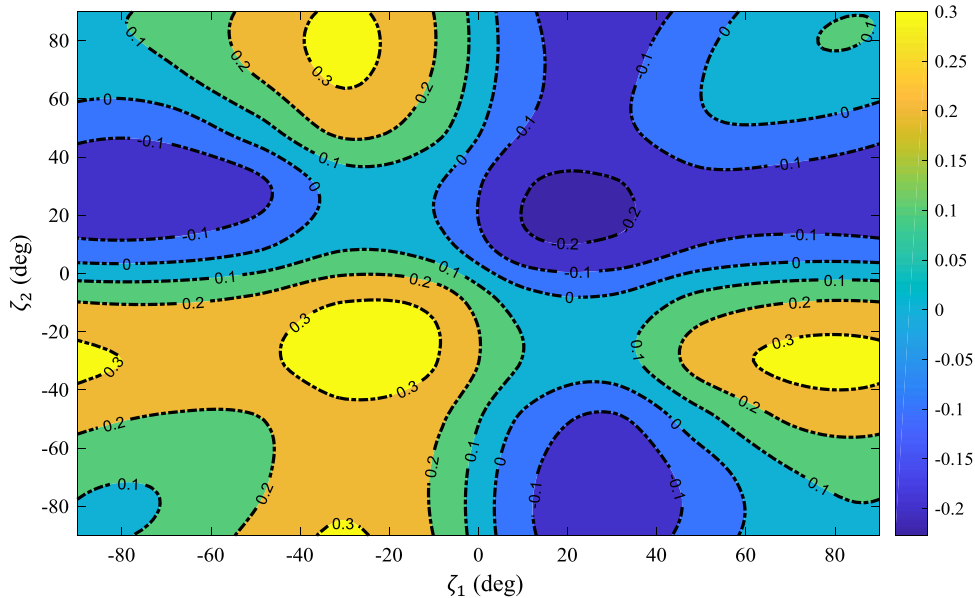

Fig. 8. Mutual effects of ζ_1 and ζ_2 on the nondimensional extension-twist coupling.

nondimensional extension-twist coupling is $-0.25 \leq \beta \leq 0.3$. This coupling is maximum in a certain range of ply angles. Some parts of this range are common with the lag-twist coupling range, and therefore during the optimization procedure this should be considered, and these regions avoided.

The skin ply angle of the cross-section not only affects the couplings, but also may change the dynamics of the blade. Therefore, in Figures 9-11, the effect of the skin ply angle on the fundamental frequencies is presented. The skin ply angle can change the lag, flap, and torsion frequencies up to 58%, 28% and 32%, respectively. In all of these plots, a certain region can be seen where the range the fundamental frequencies are close to the baseline blade. These ranges are compatible with the high lag-twist coupling range that was shown in Fig. 7. It must be pointed out here that in the range of about $-20 \leq \zeta_1, \zeta_2 \leq 20$, all the fundamental frequencies reach to their maximum value. Moreover, there are four domains located in the corners of this plot where all the fundamental frequencies

reach to their minimum values. This highlights the importance of the skin ply angle on the dynamics of the blade.

4.3. Maximizing the lag-twist coupling

In the previous section it was found that all the design variables of the blade cross-section affect the lag-twist coupling of the blade, but the skin ply angles have the highest impact. In this section a GA algorithm is used to obtain the variables so that the fundamental frequencies of the blade remain as close as possible to the baseline blade, and the lag-twist coupling reaches its highest possible value. Furthermore, the constraint on the extension-twist is also retained to minimize the effect of the centrifugal force itself on the twist distribution of the blade. Therefore, the mathematical form of the problem can be written as follows:
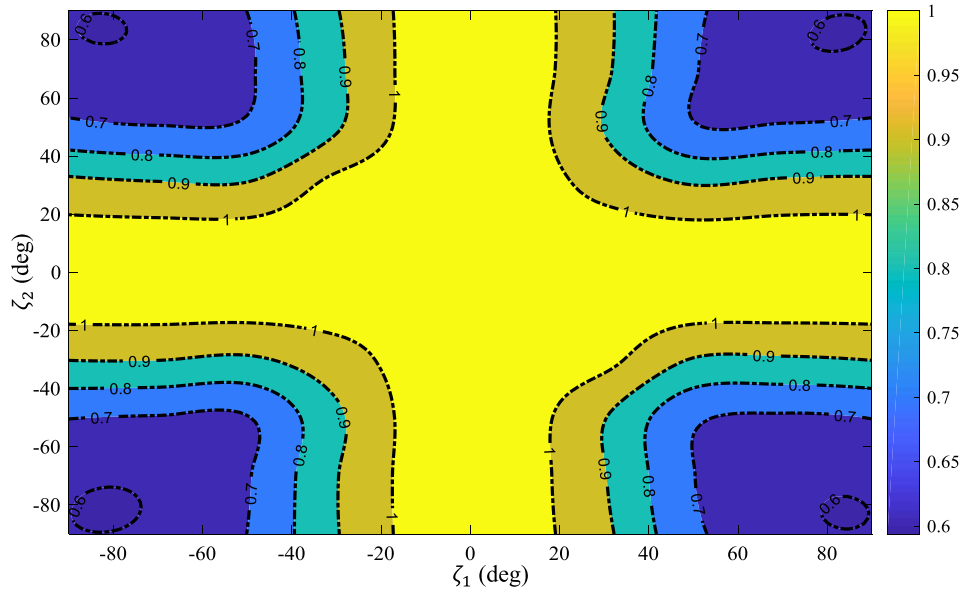
Minimize:

$$f = \frac{1}{|\alpha(\mathbf{X})|}$$

Fig. 9. The effect of ζ_1 and ζ_2 on the fundamental lag frequency (/rev).
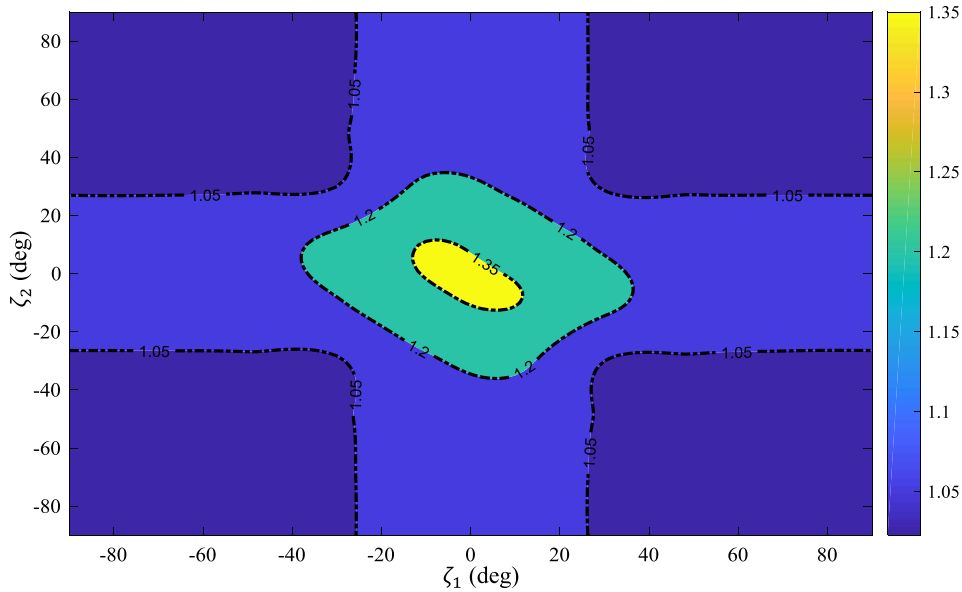

Fig. 10. The effect of ζ_1 and ζ_2 on the fundamental flap frequency (/rev).

where **X** is a column matrix containing the design variables presented in Table 1. This objective function is subjected to the following constraints:

$$\omega_{1_L}^L \leq \omega_{1_L}(\mathbf{X}) \leq \omega_{1_L}^U$$

$$\omega_{1_F}^L \leq \omega_{1_F}(\mathbf{X}) \leq \omega_{1_F}^U$$

$$\omega_{1_T}^L \leq \omega_{1_T}(\mathbf{X}) \leq \omega_{1_T}^U$$

$$\beta^L \leq |\beta(\mathbf{X})| \leq \beta^U$$

where the superscripts $(\ )^L$ and $(\ )^U$ define the lower and upper bounds of the constraints, respectively.

The best trade off design of the cross-section is presented in Table 7. With all these constraints, the highest achievable nondimensional lag-twist coupling for the proposed configuration is $\alpha = 0.44$. It is noted that the sign of the lag-twist coupling results in different twist distributions for this morphing concept, but here only the magnitude is considered.

The main cross-sectional properties of the best trade off design with respect to the leading edge of the section are presented in Table 8. It must be noted that in practice, it might not be possible to manufacture a cross-section with these optimal values due to manufacturability limitations. However, this study shows that it is possible to design a cross-section in accordance with the proposed twist morphing concept.

The effect of moving the added mass from the leading edge to the trailing edge on the twist change of the blade is shown in Fig. 12. In this case 5% mass of the blade is added to the blade and is located at the tip of the blade. It is noted that here the stiffness matrix is recalculated with respect to the shear centre of the section and the mass properties are retained to be same as the baseline blade. The solid line is the stationary blade twist distribution which is denoted as pre-twist here. The dashed line is the twist distribution of the rotating blade which is different from the pre-twist distribution. This is mainly because there are different types of couplings in the stiffness matrix. Finally, two other
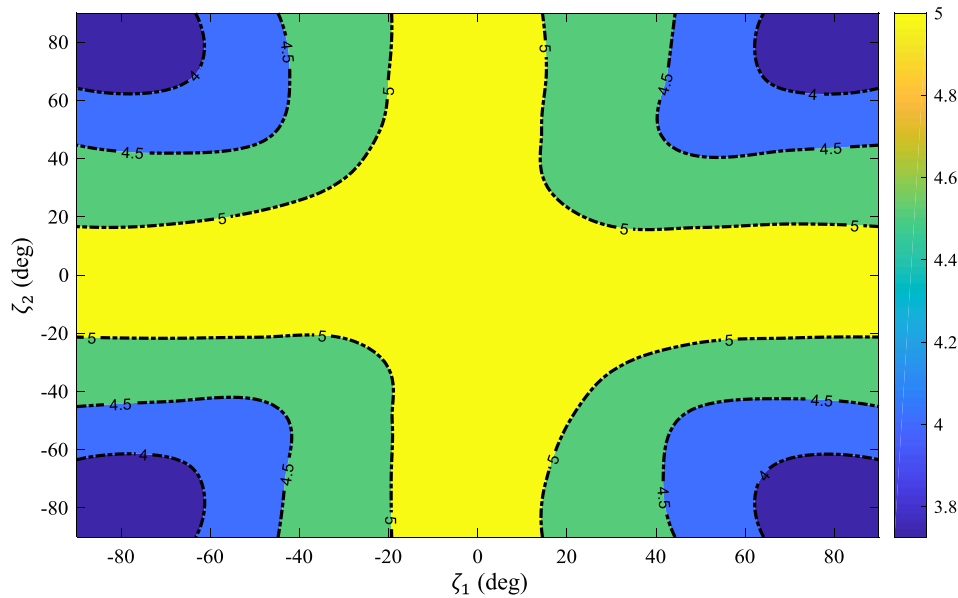
Fig. 11. The effect of ζ_1 and ζ_2 on the fundamental torsion frequency (/rev).

Table 7
Baseline and best trade off design case.

Design variable	Baseline	Optimized
ζ_1 (deg)	70°	75
ζ_2 (deg)	-83°	-39
ζ_3 (deg)	0°	27
ζ_4 (deg)	-32°	23
ζ_5 (deg)	35°	-47
ζ_6 (deg)	-70°	-57
ζ_7 (deg)	81°	29
ζ_8 (deg)	-67°	-10
ζ_9 (deg)	-26°	48
ζ_{10} (deg)	86°	-83
ζ_{11} (deg)	-73°	10
ζ_{12} (deg)	46°	73
h_{skin} (mm)	1.13	0.64
h_{spar} (mm)	5.9	3.37
y_D (mm)	-71.1	-43
ω_{L1} (/rev)	0.63	0.62
ω_{F1} (/rev)	1.04	1.03
ω_{T1} (/rev)	3.8	3.85
$|\alpha|$	0.18	0.44
$|\beta|$	0.006	0.19

Table 8
Baseline and best trade off design main cross-sectional properties.

Properties	Baseline	Optimized
S_{44} (N/m²)	1.55×10^4	9.19×10^3
S_{55} (N/m²)	7.6×10^3	3.62×10^3
S_{66} (N/m²)	2.96×10^5	3.19×10^5
S_{46} (N/m²)	-2.2×10^3	-2.36×10^4
S_{14} (N/m)	6.5×10^4	1.12×10^5
μ (kg/m)	2.76	1.43
x_{ea} (%chord)	-22	-16

Fig. 12. The effect of mass movement on the twist distribution change of the blade.

Fig. 13 shows the effect of tip added mass value ($\mu = \frac{m_p}{m}$) on the tip twist change of the blade. In this case, the tip twist change is simply the difference between the tip twist when the mass is at the leading edge and the trailing edge. By increasing the added mass value, the amount of twist change by moving the mass from the L.E. to the T.E. increases. Therefore, if a higher twist change is required, more mass should be added to the blade, or possibly the chord of the blade should be increased.

5. Conclusion

In this study, a cross-section compatible with a twist morphing concept is developed. This twist morphing concept works by moving a mass in the chordwise direction of the blade. This mass movement produces a lag bending moment on the blade that can change the twist of the blade through the lag-twist coupling. The composite blade is modelled by using the geometrically exact fully intrinsic beam equations. A parametric cross-section is introduced with different design variables. First a baseline blade which resembles the main rotor blade of the BO-105 blade is introduced. Then, the effect of different design variables of the cross-section

curves show the upper and lower bounds of twist distribution of this blade when the mass is located at the most aft or most forward positions, and the shaded area represents the domain of twist change. In this case by moving the mass from the leading edge to the trailing edge, the tip twist value of the blade changes about 5.3 deg. It must be noted that the twist distribution here is not linear.
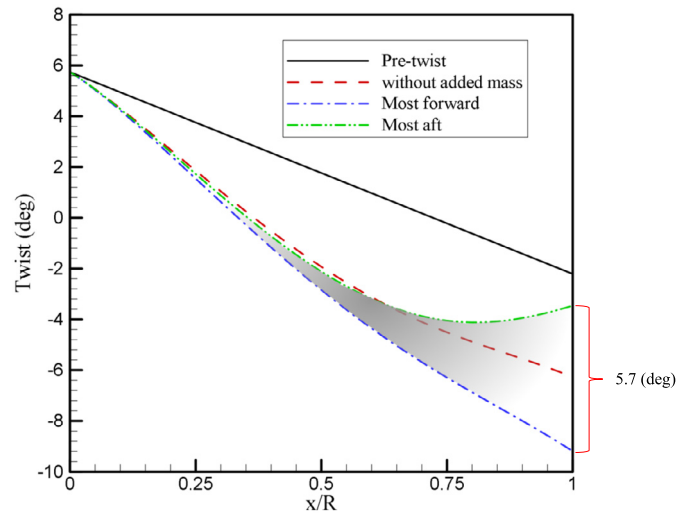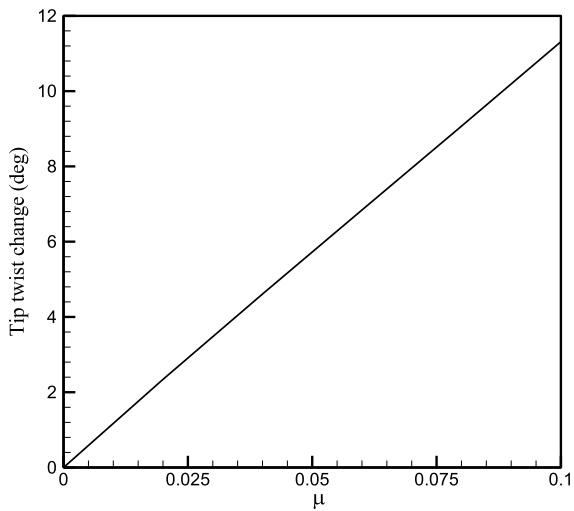
Fig. 13. The effect of the added mass value on the tip twist change of the blade.

on the lag-twist and the extension-twist coupling values were determined. It was found that the skin ply angle of the cross-section has the most contribution to both couplings. Also, the effect of the skin ply angle on the fundamental frequencies of the blade was investigated. Finally, by using the generic algorithm optimization tool, the design parameters of the cross-section were determined so that the highest possible lag-twist coupling was obtained subjected to some specific constraints. It was determined that the optimized cross-section can produce nondimensional lag-twist coupling of about 0.44 which then can produce about 5-degree tip twist change when 5% mass is added to the blade tip.

Declaration of Competing Interest

The authors declare that they have no competing interests.

Acknowledgements

References

[1] Engineering design handbook, Helicopter engineering, Part one: Preliminary design, Vol. AMCP 706-201, Headquarters, U.S. Army Material Command, Aug. 1974.

[2] D. Li, S. Zhao, A. Da Ronch, J. Xiang, J. Drofelnik, Y. Li, L. Zhang, Y. Wu, M. Kintscher, H.P. Monner, A. Rudenko, S. Guo, W. Yin, J. Kirn, S. Storm, R.D. Breuker, A review of modelling and analysis of morphing wings, Prog. Aerosp. Sci. 100 (2018) 46–62.

[3] R. Vos, Z. Gurdal, M. Abdalla, Mechanism for warp-controlled twist of a morphing wing, J. Aircr. 47 (2) (2010) 450–457.

[4] W. Raither, M. Heymanns, A. Bergamini, P. Ermanni, Morphing wing structure with controllable twist based on adaptive bending–twist coupling, Smart Mater. Struct. 22 (6) (2013) 065017.

[5] B. Jenett, S. Calisch, D. Cellucci, N. Cramer, N. Gershenfeld, S. Swei, K.C. Cheung, Digital morphing wing: active wing shaping concept using composite lattice-based cellular structures, Soft Robot. 4 (1) (2017) 33–48.

[6] P.C. Chen, I. Chopra, Induced strain actuation of composite beams and rotor blades with embedded piezoceramic elements, Smart Mater. Struct. 5 (1) (1996) 35.

[7] P.C. Chen, I. Chopra, Hover testing of smart rotor with induced-strain actuation of blade twist, AIAA J. 35 (1) (1997) 6–16.

[8] C.E.S. Cesnik, S. Shin, M.L. Wilbur, Dynamic response of active twist rotor blades, Smart Mater. Struct. 10 (1) (2001) 62.

[9] S.J. Shin, C. Cesnik, Forward flight response of the active twist rotor for helicopter vibration reduction, in: 19th AIAA Applied Aerodynamics Conference, American Institute of Aeronautics and Astronautics, 2001.

[10] D. Thakkar, R. Ganguli, Helicopter vibration reduction in forward flight with induced-shear based piezoceramic actuation, Smart Mater. Struct. 13 (3) (2004) 599.

[11] H. Prahlad, I. Chopra, Design of a variable twist tilt-rotor blade using shape memory alloy (SMA) actuators, in: SPIE's 8th Annual International Symposium on Smart Structures and Materials, 2001.

[12] G.S. Bushnell, D. Arbogast, R. Ruggeri, Shape control of a morphing structure (rotor blade) using a shape memory alloy actuator system, in: Proceedings of SPIE Smart Structures and Materials, 2008.

[13] A. Pagano, S. Ameduri, V. Cokonaj, A. Prachar, Z. Zachariadis, D. Drikakis, Helicopter blade morphing strategies aimed at mitigating environmental impact, J. Theor. Appl. Mech. 49 (4) (2011) 1233–1259.

[14] M. Mistry, F. Gandhi, M. Nagelsmit, Z. Gurdal, Actuation requirements of a warp-induced variable twist rotor blade, J. Intell. Mater. Syst. Struct. 22 (9) (2011) 919–933.

[15] D. Han, V. Pastrikakis, G.N. Barakos, Helicopter flight performance improvement by dynamic blade twist, Aerosp. Sci. Technol. 58 (2016) 445–452.

[16] M.R. Amoozgar, A.D. Shaw, J. Zhang, M.I. Friswell, Twist morphing of a hingeless rotor blade using a moving mass, in: Proceedings of the 44th European Rotorcraft Forum, Delft, 2018.

[17] M.R. Amoozgar, A.D. Shaw, J. Zhang, M.I. Friswell, Composite blade twist modification by using a moving mass and stiffness tailoring, AIAA J. (December 2018), https://doi.org/10.2514/1.J057591, in press.

[18] M.R. Amoozgar, A.D. Shaw, J. Zhang, M.I. Friswell, The effect of a movable mass on the aeroelastic stability of composite hingeless rotor blades in hover, J. Fluids Struct. 87 (2019) 124–136.

[19] E.C. Smith, I. Chopra, Formulation and evaluation of an analytical model for composite box-beams, J. Am. Helicopter Soc. 36 (3) (1991) 23–35.

[20] L. Li, V.V. Volovoi, D.H. Hodges, Cross-sectional design of composite rotor blades, J. Am. Helicopter Soc. 53 (3) (2008) 240–251.

[21] C.E.S. Cesnik, J. Mok, J.A. Morillo, A.S. Parikh, Design optimization of active twist rotor blades, in: Proceedings of the 30th European Rotorcraft Forum, Marseilles, 2004.

[22] B. Glaz, P. Friedmann, L. Liu, D. Kumar, C. Cesnik, The AVINOR aeroelastic simulation code and its application to reduced vibration composite rotor blade design, in: 50th AIAA/ASME/ASCE/AHS/ASC Structures, Structural Dynamics, and Materials Conference, 2009.

[23] R. Ganguli, I. Chopra, Aeroelastic optimization of a helicopter rotor with two-cell composite blades, AIAA J. 34 (4) (1996) 835–841.

[24] V. Volovoi, S. Yoon, C.-Y. Lee, D. Hodges, Structural optimization of composite rotor blades, in: 45th AIAA/ASME/ASCE/AHS/ASC Structures, Structural Dynamics & Materials Conference, American Institute of Aeronautics and Astronautics, 2004.

[25] J. Paik, V. Volovoi, D. Hodges, Cross-sectional sizing and optimization of composite blades, in: 43rd AIAA/ASME/ASCE/AHS/ASC Structures, Structural Dynamics, and Materials Conference, American Institute of Aeronautics and Astronautics, 2002.

[26] V. Volovoi, L. Li, J. Ku, D. Hodges, Multi-level structural optimization of composite rotor blades, in: 46th AIAA/ASME/ASCE/AHS/ASC Structures, Structural Dynamics and Materials Conference, American Institute of Aeronautics and Astronautics, 2005.

[27] V. Volovoi, J. Ku, D. Hodges, Coupling global and local aspects of cross-sectional optimization for rotor blades, in: 47th AIAA/ASME/ASCE/AHS/ASC Structures, Structural Dynamics, and Materials Conference, American Institute of Aeronautics and Astronautics, 2006.

[28] N.A. Vu, J.W. Lee, T.P.N. Le, S.T.T. Nguyen, A fully automated framework for helicopter rotor blades design and analysis including aerodynamics, structure, and manufacturing, Chin. J. Aeronaut. 29 (6) (2016) 1602–1617.

[29] W. Yu, D.H. Hodges, V. Volovoi, C.E.S. Cesnik, On Timoshenko-like modeling of initially curved and twisted composite beams, Int. J. Solids Struct. 39 (19) (2002) 5101–5121.

[30] D.H. Hodges, Geometrically exact, intrinsic theory for dynamics of curved and twisted anisotropic beams, AIAA J. 41 (6) (2003) 1131–1137.

[31] M. Amoozgar, H. Shahverdi, Dynamic instability of beams under tip follower forces using geometrically exact, fully intrinsic equations, Lat. Am. J. Solids Struct. 13 (2016) 3022–3038.

[32] M.R. Amoozgar, H. Shahverdi, Analysis of nonlinear fully intrinsic equations of geometrically exact beams using generalized differential quadrature method, Acta Mech. 227 (5) (2016) 1265–1277.

[33] M.R. Amoozgar, H. Shahverdi, A.S. Nobari, Aeroelastic stability of hingeless rotor blades in hover using fully intrinsic equations, AIAA J. 55 (7) (2017) 2450–2460.

[34] C. Sachdeva, M. Gupta, D.H. Hodges, Modeling of initially curved and twisted smart beams using intrinsic equations, Int. J. Solids Struct. 148–149 (2017) 3–13.

[35] Z. Sotoudeh, D.H. Hodges, Structural dynamics analysis of rotating blades using fully intrinsic equations, Part I: Formulation and verification of single-load-path configurations, J. Am. Helicopter Soc. 58 (3) (2013) 1–9.